Chemical Engineering Journal 157 (2010) 323–330

Contents lists available at ScienceDirect

Chemical Engineering Journal

journal homepage: www.elsevier.com/locate/cej

Selective deposition of fine particles in constant-flux submerged membrane filtration

Kuo-Jen Hwang*, Hsieng-Chia Chen

Department of Chemical and Materials Engineering, Tamkang University, Tamsui, Taipei Hsien 25137, Taiwan

ARTICLE INFO

Article history:
Received 6 June 2009
Received in revised form 2 November 2009
Accepted 4 November 2009

Keywords:
Microfiltration
Submerged membrane filtration
Particle deposition
Cake properties
Particle size distribution

ABSTRACT

The selective deposition of fine particles in a constant-flux submerged microfiltration system is studied. The effects of operating conditions, such as filtration flux, injected air flow rate and air bubble size, on the particle deposition probability, cake mass and average specific cake filtration resistance are discussed. Smaller particles have more opportunity to deposit onto the membrane surface. The particle size distribution in the filter cake increases with increasing the filtration flux or bubble size, but with decreasing the injected air flow rate. The external forces exerted on the depositing particles are analyzed based on hydrodynamics and DLVO theory. The drag forces due to suspension flow, permeate flow, and bubble flow play the major role in determining the particle stability on the membrane surface. Interparticle forces are dominant for submicron particles, while gravitational force increases its weight as particle size exceeds 5 μm. A force balance model is used for estimating the particle deposition probability. An increase in filtration flux or a decrease in air flow rate leads to higher particle deposition probability, heavier cake, or lower average specific cake filtration resistance. The deposition probability is higher by injecting bigger bubbles under a specified air flow rate due to the lower bubble generation frequency. Consequently, a decrease in bubble size causes to lighter cake but higher average specific filtration resistance. The validities of the model predictions for particle deposition probability, cake mass and average specific filtration resistance are demonstrated by experimental data.

1. Introduction

Submerged membrane filtration has been increasingly used in membrane bioreactor and wastewater treatment processes in recent years. Since it can be integrated with chemical or bioreactors and be operated at high filtration rate for a long time, this kind of filtration has attracted not only process engineers but also researchers in the related fields. However, the membrane fouling due to particle deposition or molecular adsorption is still the most serious problem in industrial operations. Therefore, how to improve its performance by reducing particle fouling is one of the essential courses to faster develop an efficient submerged membrane filtration system.

Several methods have been proposed to reduce particle fouling in microfiltration and ultrafiltration, such as increasing fluid tangential velocity, periodical backwash, sparging air bubbles or introduce turbulent flow, etc. [1]. In a submerged membrane filtration system, the membrane fouling is mainly determined by the hydrodynamic conditions, *e.g.*, filtration pressure, aeration intensity, bubble flow pattern, etc. [2–4]. Chang and Fane [5] and Fane et al. [6] discussed the effects of fiber diameter, module design and operating conditions on the filtration flux in the submerged hollow fiber filtration of yeast cells. The introduced air-bubbles flowing among hollow fibers effectively restrained the membrane fouling. They concluded that the bubble flow pattern and liquid–gas flow rate ratio were important factors on the membrane fouling and increasing shear stress by sparging air bubbles was an efficient way to enhance filtration flux. Hwang and Chen [4] studied the particle fouling in a constant-pressure submerged ceramic membrane filtration. The critical condition for particle deposition was discussed using a force balance model. They concluded that an increase in air flow rate led to less cake accumulation, but increasing filtration pressure contrarily resulted in more serious membrane pore blocking and lower filtration flux. Therefore, to understand the effects of air injection rate, air bubble size and filtration flux on the particle deposition becomes an essential step to achieve an optimum system design.

Although many researches focused on the membrane fouling in microfiltration or ultrafiltration, most of them considered uniform-size particles. For a particulate sample with a wide-size distribution, its filterability is far different from a uniform-size one even having the same mean particle size [7–9]. In addition, a few

* Corresponding author. Tel.: +886 2 26215656x2726; fax: +886 2 26209887.
E-mail address: kjhwang@mail.tku.edu.tw (K.-J. Hwang).

1385-8947/$ – see front matter © 2009 Elsevier B.V. All rights reserved.
doi:10.1016/j.cej.2009.11.008

Nomenclature

C_1	correction factor of drag force due to suspension flow
C_2	correction factor of drag force due to permeate flow
C_3	constant defined in Eq. (6)
C_4–C_5	constants defined in Eq. (10)
C_D	drag coefficient
C_b	particle concentration in suspension (kg/m^3)
d_b	bubble diameter (m)
d_p	particle diameter (m)
D	equilibrium distance between particles (m)
$f_c(d_p)$	frequency function of size d_p in cake
$f_o(d_p)$	frequency function of size d_p in suspension
F_b	drag force due to bubble flow (N)
F_g	gravitational force (N)
F_i	net interparticle force (N)
F_l	inertial lift force (N)
F_p	drag force due to permeate flow (N)
F_t	drag force due to suspension flow (N)
f_r	bubble generation frequency (s^{-1})
k	Kozeny constant
L	cake thickness (m)
N_b	mass flux of particles arriving at the membrane surface (kg/m^2 s)
N_w	mass flux of particle deposition (kg/m^2 s)
$P(d_p)$	probability of particle deposition
Q_b	air volumetric flow rate (m^3/s)
q	filtration flux (m^3/m^2 s)
R_t	total filtration resistance (m^{-1})
S_o	specific surface area of particles (m^2/m^3)
t	filtration time (s)
u_b	bubble rising velocity (m/s)
u_p	undisturbed fluid velocity at the particle center (m/s)
V_b	volume of a single bubble (m^3)
v_l	lift velocity of particles (m/s)
w_c	cake mass per unit filtration area (kg/m^2)

Greek letters

α_{av}	average specific cake filtration resistance (m/kg)
δ	thickness of Stern layer (m)
ε	average cake porosity
ε_o	porosity of the most compact cake
γ_w	shear rate at the membrane surface (1/s)
μ	fluid viscosity (kg/m s)
ν	fluid kinematic viscosity (m^2/s)
ρ	liquid density (kg/m^3)
ρ_b	bubble density (kg/m^3)
ρ_s	particle density (kg/m^3)
τ_b	shear stress acting by rising bubbles (N/m^2)
τ_w	shear stress acting on the membrane surface (N/m^2)

researchers analyzed the critical conditions of particle deposition on the membrane surface using moment balance [7] or force balances [8,9]. The critical (largest) diameter for particle deposition could be expressed as a function of operating conditions. However, the particles considered in those studies were all in micron size. Since the external forces have different weights for micron and submicron particles, the previous models should be modified for wide-size-distributed particles. Recently, Hwang et al. [10] studied the particle size effect on the particle deposition in a two-parallel-plate cross-flow microfiltration. The particle deposition probability could be explained by the force analysis based on hydrodynamics.

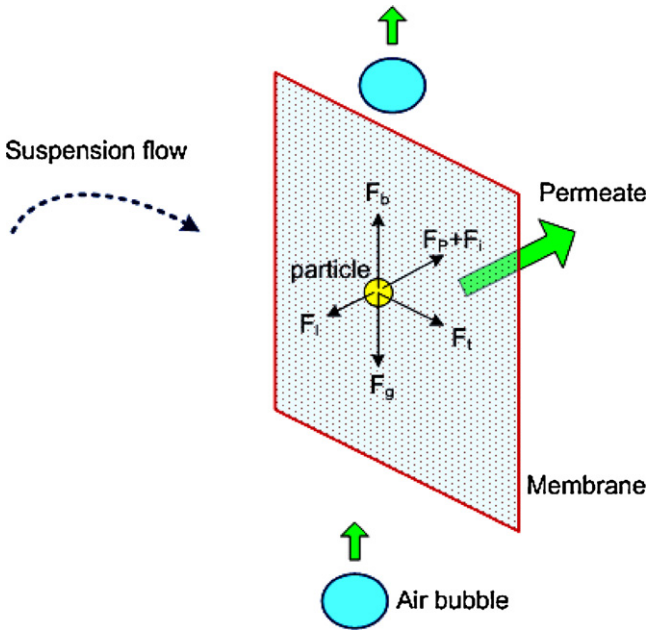

Fig. 1. Forces analysis on a depositing particle in the submerged membrane filtration.

In this article, the effects of particle size, filtration flux, air flow rate and bubble size on the particle deposition, cake mass and average specific cake filtration resistance in a submerged membrane filtration system are studied. A particulate sample with a size distribution ranging from submicron to micron is filtered using a flat-sheet membrane module. The particle deposition probabilities under various conditions are analyzed using a force balance model based on hydrodynamics and DLVO theory. The cake properties are calculated theoretically and compared with experimental data.

2. Particle deposition model

2.1. Force analysis on a depositing particle

Fig. 1 shows a schematic diagram of the forces exerted on a depositing particle in the submerged membrane filtration. A flat-sheet membrane module is submerged vertically in a suspension tank with mechanical mixing and air bubble injection. Particles are transported by the fluid flow, and some of them may have opportunity to arrive at the membrane surface during a filtration. The external forces exerted on a depositing particle staying on the membrane surface include the drag forces due to the suspension flow, F_t, and the permeate flow, F_p, the inertial lift force, F_l, the net gravitational force (gravitational force minus buoyant force), F_g, the net interparticle force, F_i, and the shear force due to bubble flow, F_b, as indicated in Fig. 1. The particle would be more stable under larger values of F_p or attractive F_i, but may be swept away from the membrane surface if other forces play the major roles. Therefore, whether the particle can deposit stably or not is determined by the resultant external forces. The forces are analyzed as follows.

2.1.1. Drag force due to suspension flow

In the system shown in Fig. 1, the suspension flows tangentially across the membrane surface due to a mechanical agitation. The tangential drag force acting on the particle can be estimated by the modified Stokes law since the local fluid velocity in the boundary layer on the membrane surface is very low, that is,

$$F_t = 3\pi\mu d_p u_p C_1 \quad (1)$$

where μ is the fluid viscosity, d_p is the particle diameter, u_p is the undisturbed fluid velocity at the particle center, and C_1 is a correction factor due to the presence of the membrane and cake. Although the fluid flow field has a velocity distribution (it was measured using a Pitot tube in this study), it is reasonable to consider the velocity profile very close to the membrane surface is linear. Consequently, the value of C_1 is equal to 1.7009 [11].

2.1.2. Drag force due to permeate flow

Because the Reynolds number in the filtration direction is very small under most conditions, the drag force due to permeate flow can also be calculated by the modified Stokes law, that is,

$$F_p = 3\pi\mu d_p q C_2 \tag{2}$$

where q is the filtration flux. The correction factor, C_2, due to the existences of the membrane and cake can be estimated using the following equation [12]:

$$C_2 = 0.36\left(\frac{R_t d_p^2}{4L}\right)^{2/5} \tag{3}$$

where L is the cake thickness, and R_t is the overall filtration resistance which is the summation of the cake and membrane resistances. The cake thickness can be calculated using a material balance once the cake mass and porosity are measured.

2.1.3. Inertial lift force

The inertial lift force is weighty in determining particle deposition only when large particles are under high shear rate [4,6]. The inertial lift velocity of particles in a linear tangential flow pattern can be calculated by [13]

$$v_l = \left(\frac{61\gamma_w^2}{576\nu}\right)\cdot\left(\frac{d_p}{2}\right)^3 \tag{4}$$

where ν is the fluid kinematic viscosity and γ_w is the shear rate at the membrane surface. Thus, the inertial lift force can be estimated by substituting the v_l value into the modified Stokes law.

2.1.4. Net gravitational force

The net gravitational force exerted on a submerged particle can be given by

$$F_g = \frac{\pi}{6}(\rho_s - \rho)g d_p^3 \tag{5}$$

where ρ_s and ρ are the densities of particle and fluid, respectively.

2.1.5. Net interparticle force

The interparticle forces are dominant for submicron particles. According to the DLVO theory, the major interparticle forces include the van der Waals force and electrostatic force, and the net interparticle force can be calculated by summing these forces. The detail calculation procedures can refer to the author's previous study [14].

2.1.6. Shear force due to bubble flow

The modified Stokes law for drag force estimation can be rewritten as [4]:

$$F_b = C_3 d_p^2 \tau_w \tag{6}$$

where τ_w is the shear stress acting on the membrane surface, and C_3 is a constant. The shear stress produced by rising bubbles can be considered to be proportional to the shear stress acting on the bubble surface, τ_b, and the bubble generation frequency, f_r [4]. According to the definition of drag coefficient, C_D, the shear stress acting on the bubble surface can be calculated by

$$\tau_b = C_D\left(\frac{\rho_b \cdot u_b^2}{2}\right) \tag{7}$$

where ρ_b and u_b are the bubble density and rising velocity, respectively. For a single air bubble of negligible density, the drag coefficient is commonly evaluated by [15]:

$$C_D \equiv \frac{4gd_b}{3u_b^2} \tag{8}$$

where d_b is the bubble equivalent diameter. Therefore, the value of τ_b can be calculated using Eq. (7) once the bubble diameter and rising velocity are measured. On the other hand, the bubble generation frequency can be calculated by

$$f_r = \frac{Q_b}{V_b} = \frac{6Q_b}{\pi d_b^3} \tag{9}$$

where Q_b is the air volumetric flow rate, and V_b is the volume of a single bubble. The relationship between d_b and Q_b can be measured in experiments or directly obtained by a dimensional analysis [15].

Therefore, the shear force due to bubble flow can be estimated by substituting Eqs. (7)–(9) into Eq. (6), that is

$$F_b = C_4 d_p^2 \cdot \tau_b \cdot f_r = C_5 \frac{\rho_b d_p^2 Q_b}{d_b^2} \tag{10}$$

The coefficient C_5 can be obtained by regressing experimental data under the condition at which a particle with a diameter of d_p can just stably deposit [4].

2.2. Particle deposition on the membrane surface

2.2.1. Particle deposition model

A force balance model is used in this study to determine the critical conditions of particle deposition [8,10]. This method is concisely described as below. When a depositing particle approaches a stably deposited particle on the cake surface, the external forces are analyzed and divided into vectors in two directions which are vertical (tangential direction) and parallel (normal direction), respectively, to the connected line between two particle centers. The particles are separated with an equilibrium distance if the net normal force is repulsive. Otherwise, the particles are in contact with each other if the net normal force is attractive.

In the condition of repulsive net normal force, particles cannot actually contact with each other. The lubricant effect due to electric double layer causes the depositing particle to migrate along the net tangential force direction. In other words, whether the particle can deposit or not is determined by the net tangential force direction. In contrast, the particles will contact with each other under the attractive net normal force condition. In such a condition, the particle can deposit stably when the friction force (the product of normal force and particle friction coefficient) is larger than the tangential force. The critical friction angle between particles, defined as the largest particle contact angle for stable deposition, is therefore estimated based on this concept [8,10,14].

2.2.2. Probability of particle deposition

The particle deposition probability on the membrane surface can be theoretically considered as the fraction of the area for stable deposition to the total providing area. The detail calculation procedures can refer to the authors' previous studies [8,10,14]. Those analyses indicated that the particle deposition probability is a function of particle size and operating conditions.

On the other hand, the particle deposition probability can also be obtained from experimental data. Making a particle balance for

those arriving at the membrane surface, the particle deposition probability can be expressed as [7,8,10]:

$$P(d_p) = \frac{f_c(d_p)N_w}{f_o(d_p)N_b} \tag{11}$$

where $f_c(d_p)$ and $f_o(d_p)$ are the frequency functions of the particles with a diameter of d_p in the cake and the suspension, respectively. The particle mass flux arriving at the membrane surface, N_b, can be calculated by the product of suspension concentration and filtration flux by assuming uniformly dispersed suspension, while the mass flux of particle deposition, N_w, can be obtained from the time differentiation of the cake accumulation curve.

2.3. Cake properties

The important cake properties include mass, porosity, particle size distribution and specific filtration resistance. They can be measured in experiments or calculated theoretically. The calculation methods are described as follows.

Once the deposition probability for each particle size is obtained, the cake mass grew within a time interval can be calculated by the following integration:

$$w_c = \int_0^t C_b \cdot q \cdot \left(\int_0^\infty f_o(d_p) \cdot P(d_p) dd_p \right) dt \tag{12}$$

where w_c is the cake mass per unit filtration area, C_b is the suspension concentration, and t is filtration time.

A free cell model for particle packing in a filter cake was proposed by Hwang et al. [14]. According to the cell model, the cake porosity can be estimated as following:

$$\varepsilon = 1 - (1 - \varepsilon_o) \cdot \left(\frac{d_p + 2\delta}{d_p + D} \right)^3 \tag{13}$$

where ε is the cake porosity, δ is the Stern layer thickness, D is the equilibrium distance between neighbor particles, and ε_o is the porosity of the most compact cake which ranges from 0.38 to 0.43 [14].

Comparing the basic filtration equation and the Kozeny equation, the average specific cake filtration resistance can be calculated using the following equation:

$$\alpha_{av} = \frac{kS_o^2(1-\varepsilon)}{\rho_s \varepsilon^3} \tag{14}$$

where k is the Kozeny constant, and S_o is the specific surface area of particles. For spherical particles under a compact packing, the k value is equal to 5.0. The specific surface area of particles is equal to $6/d_p$ for a spherical particle with a diameter of d_p. When particles have a size distribution, the S_o value can be estimated using the mean particle diameter. Therefore, the average specific cake filtration resistance can be theoretically calculated using Eq. (14) once the values of kS_o^2 and ε are known.

3. Materials and methods

Spherical particles made of polymethyl methacrylate (PMMA) were purchased from Soken Chemical & Engineering Co. in Japan (catalog number: MR-7G) and used in experiments. The particle density and mean diameter were 1210 kg/m^3 and 7.0 μm, respectively. Most particles had diameters ranging from 0.2 to 20 μm, and the original particle size distribution will be shown later (Fig. 5). The particles were hydrophilic and were suspended in de-ionized water to prepare a 0.1 wt% suspension. The suspension pH and temperature were kept at 7.0 and 20 °C, respectively, during filtration. The particle zeta potential in such a condition was measured as −25.2 mV. No particle coagulation was observed in such a condition. The filter membrane used in experiments was made of mixed cellulose ester and manufactured by ADVANTEC Micro Filtration Systems in Japan. The mean pore size and thickness of the membrane were 0.1 and 125 μm, respectively. The clean membrane filtration resistance was 2.52×10^{11} m^{-1} under a pressure of 80 kPa.

Before filtration, PMMA particles were slowly added into de-ionized water to prepare a 10-l 0.1 wt% suspension. The suspension was poured into an 18.85 cm-diameter cylindrical suspension tank after 30 min dispersion using ultrasonication. Filter membrane was fixed on an acrylic flat-sheet filter module, which was installed vertically at a distance of 4.3 cm from the tank axial line and 7.0 cm from the tank bottom. The filtration area was rectangular in shape with a width of 2.88 cm and a height of 0.96 cm. The suspension was agitated continuously using a mechanical mixer. The rotation speed of the mixer was fixed at 300 rpm during filtration. Since no baffle was used in the tank, the suspension flowed across

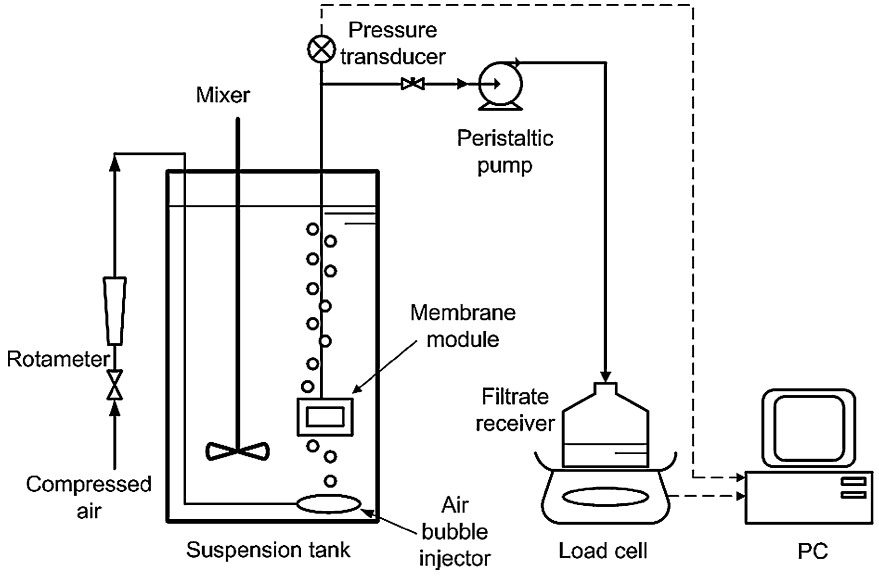

Fig. 2. A schematic diagram of the submerged membrane filtration system.

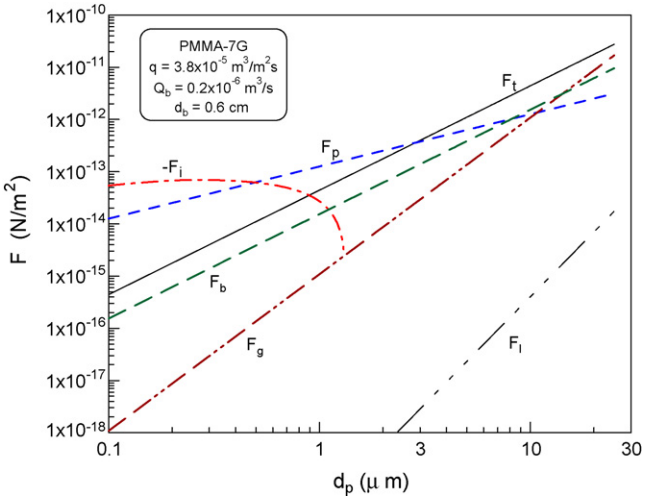

Fig. 3. Forces exerted on particles with various diameters.

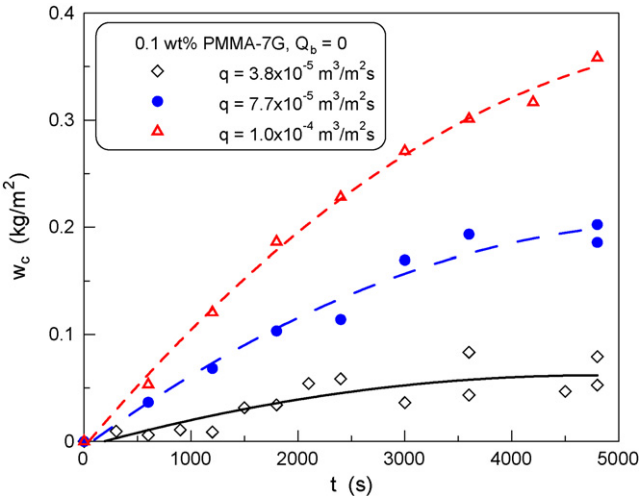

Fig. 4. Time courses of cake mass under various filtration fluxes.

the filter module horizontally. The velocity profile near the membrane surface was measured using a Pitot tube. Thus, the shear stress on the membrane surface due to suspension flow can be calculated accordingly. Constant-flux filtration experiments were carried out using the filtration system shown in Fig. 2. The filtration flux was controlled using a digital peristaltic pump. Three constant fluxes were used in experiments, they are 3.8×10^{-5}, 7.7×10^{-5} and 1.0×10^{-4} m^3/m^2s, respectively. The transmembrane pressure was recorded during the filtration by a personal computer through a pressure transducer. Compressed air was injected into the suspension tank through an air bubble injector which was put under the filter module at a distance of 2.0 cm. The air flow rate ranged from 0 to 9×10^{-7} m^3/s in this study. The injector's head was exchangeable and designed to generate fixed-size air bubbles one by one. The bubble generation frequency was determined by the injector size and the air flow rate which was controlled and measured using a rotameter. The air flow pattern was captured by a digital camera through the transparent tank wall, and the air bubble size was analyzed using a *Power Image Analysis System*. When a filtration was terminated, the filter module was taken out from the suspension tank. The cake formed on the filter membrane was scraped down and sent to analyze its wet and dry masses using an *ORION* moisture titrator and the particle size distribution using a *HORIBA LA-910* particle sizer. The average cake porosity and average specific cake filtration resistance could then be calculated by a material balance and the basic filtration equation, respectively.

4. Results and discussion

Fig. 3 shows the external forces exerted on depositing particles with different diameters under $Q_b = 0.2 \times 10^{-6}$ m^3/s and $q = 3.8 \times 10^{-5}$ m^3/m^2 s. The shear rate γ_w due to suspension flow and the coefficient C_5 in Eq. (10) were measured as 28.34 s^{-1} and 17.04 m/s, respectively, under the agitation condition of this study. The Hamaker constant for van der Waals force calculation was 1.05×10^{-20} J [16], and the particle zeta potential was measured as −25.2 mV. The net interparticle force was calculated using DLVO theory and thus obtained by summing van der Waals and electrostatic forces. The net interparticle force shown in Fig. 3 is repulsive (minus) for a submicron particle, while becomes attractive as particle size exceeds 1 μm. The curves in Fig. 3 show that the drag forces increase with increasing particle size and indeed play the major role on particle deposition. The net interparticle force is dominant for submicron particles, while the gravitational force becomes weighty for particles larger than 5 μm. All major forces have the same order of magnitude when particle size exceeds 10 μm, while the inertial lift force is negligible compared to the others in the operating conditions of this study. These results imply that particle size is an important factor affecting particle deposition.

Fig. 4 shows the time courses of cake mass under various filtration fluxes. The cake mass linearly increases with time in the early period of filtration under a constant flux. This indicates a constant particle deposition rate occurring at that time. However, the cake accumulation rate gradually decreases after 2000 s. The decrease in particle deposition probability is attributed to the variations of external forces even under a constant flux. In fact, the drag force exerted on depositing particles due to permeate flow may decrease continuously during a filtration because of the decrease in deposited particle size as well as the correction factor C_2 in Eq. (2). Furthermore, a higher filtration flux leads to a heavier cake, as shown in Fig. 4. It can be expected because an increase in filtration flux causes a higher transported particle flux arriving at the membrane surface and a larger drag force due to permeate flow.

Fig. 5 depicts the particle size distributions in the cake under various filtration fluxes and no air bubble injection. The original particle size distribution in the suspension is also shown as the solid curve for comparison. The particle size distributions in cake

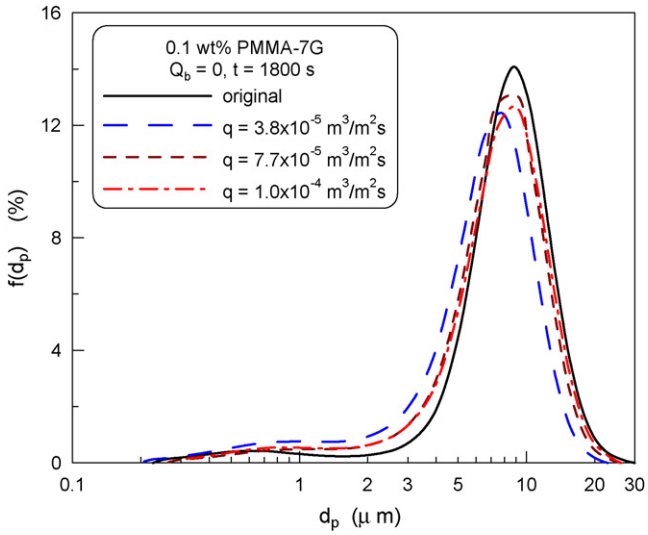

Fig. 5. Effect of filtration flux on the particle size distribution in cake.

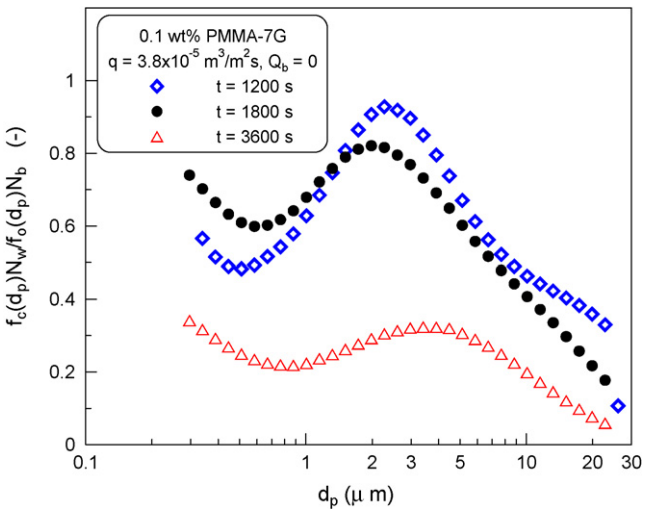

Fig. 6. Effect of particle size on the deposition probability at three filtration times.

are measured at 1800 s, and they are all smaller than that in the original suspension. This is because the particle deposition probability strongly depends on their size and, generally, small particles are more stable staying on the membrane surface on the viewpoint of hydrodynamics [8,10]. The data shown in Fig. 5 clearly indicates that the particle size distribution increases with increasing filtration flux. The particle size distribution is closer to the original under higher filtration flux due to the increase in particle stability.

Fig. 6 is a plot of $f_c(d_p)N_w/f_o(d_p)N_b$ versus d_p at three different filtration times. The filtration flux was fixed at 3.8×10^{-5} m^3/m^{2}s, and no air bubble was injected. As mentioned previously, the value of $f_c(d_p)N_w/f_o(d_p)N_b$ can be considered as the deposition probability of particles with a diameter of d_p. The curves show an interesting trend which is quite different from those in previous studies [7–9]. A critical diameter for particle deposition was observed [7–9], and the particles which size exceeds the critical value cannot stably deposit onto the membrane surface. However, in this study, the particle deposition probability decreases with particle size in the submicron region and reaches a minimum value at *ca.* 0.6 μm, and then increases continuously until a maximum probability occurring at 3–5 μm. The deposition probability decreases quickly after it attains the maximum. Comparing the values of particle deposition probability at different times, the probability for a given particle size decreases with filtration time. For example, the deposition probability is as high as 0.85 at 1200 s for a 3-μm particle, while it drops to 0.30 at 3600 s. The significant decrease in deposition probability after 1800 s causes the particle deposition to be more difficult. No wonder the cake accumulation rate decreases gradually after 2000 s, as shown in Fig. 4.

Fig. 7 shows comparisons of particle deposition probability between calculated results and experimental data under various filtration fluxes. All calculated curves have the same tendency and can be explained by the force analysis. In the submicron region, the electrostatic and van der Waals forces are dominant. The repulsive net interparticle force causes particles to separate with their neighbors. Since the drag force due to permeate flow (F_p) is offset by the net interparticle force, a larger particle may have a lower deposition probability due to larger drag force causing by the tangential suspension flow (F_t). When particle size exceeds 1 μm, the net interparticle force changes to be attractive, this causes particles to contact with their neighbors and results in higher particle deposition probability. However, the value of F_t surpasses F_p at the particle size *ca.* 2–3 μm. This makes larger particles to be more unstable, and a decrease in deposition probability with particle size can then be observed. When particle size exceeds 5 μm, the gravitational force (F_g) becomes weighty, while the net interparticle force is contrarily trivial. Since the net tangential force is the resultant force of F_t and F_g (F_l is negligible), the increase in F_g may vary the direction and magnitude of the net tangential force. Consequently, the decay of deposition probability becomes slower as particle size is greater than 5 μm. Moreover, the impact of F_p becomes much lower than those of F_t and F_g when particle size exceeds 10 μm, as shown in Fig. 3. This leads to similar calculated deposition probability for a given particle size even under different filtration fluxes. Comparing the results shown in Fig. 7, the deposition probability increases with increasing filtration flux. However, the data for those two higher fluxes are very close. In fact, the deposition probability is lower under $q = 1.0 \times 10^{-4}$ m^3/m^{2}s when particle diameter exceeds 3 μm. This is because of the similar resulting drag forces in the filtration direction. A higher flux causes to a thicker cake and, therefore, to a smaller correction factor C_2 in Eq. (2). In addition, overestimates in $P(d_p)$ in the submicron-size region are obtained. This is possible due to the neglect of particle diffusion in the deposition model. Since the diffusion effect is more significant for smaller submicron particles, considerable deviations as large as 30% occur for the smallest particles. The other possibility is the measured errors causing by few submicron particles existing in the suspension as well as in the filter cake. The comparison shown in Fig. 7 also indicates that the particle deposition probability can be predicted appropriately using the proposed model except under a low filtration flux, e.g., $q = 3.8 \times 10^{-5}$ m^3/m^{2}s. Since the trends of calculated results and experimental data are similar, the deviation between them is reasonably attributed to the overestimation in the total cake mass. The cake formed under such a low flux is possibly affected by the suspension flow pattern. In other words, the particle mass flux arriving at the membrane surface may be less than that estimated by a material balance in the "dead-end" cake filtration. As a result, a 2-fold overestimation in $P(d_p)$ is found in such a condition.

Air bubbles with specified sizes under various flow rates were injected into the suspension tank to study the effect of air-sparging on the particle deposition in a submerged membrane filtration. Two bubble sizes were selected in the experiments; they are 0.45 and 0.60 cm, respectively. Fig. 8 shows the effects of bubble size and air flow rate on the particle deposition probability under a fixed filtration flux of 7.7×10^{-5} m^3/m^{2}s. The symbols shown in figure are experimental data, while the curves are the calculated results using the proposed model. The comparison indicates that the model

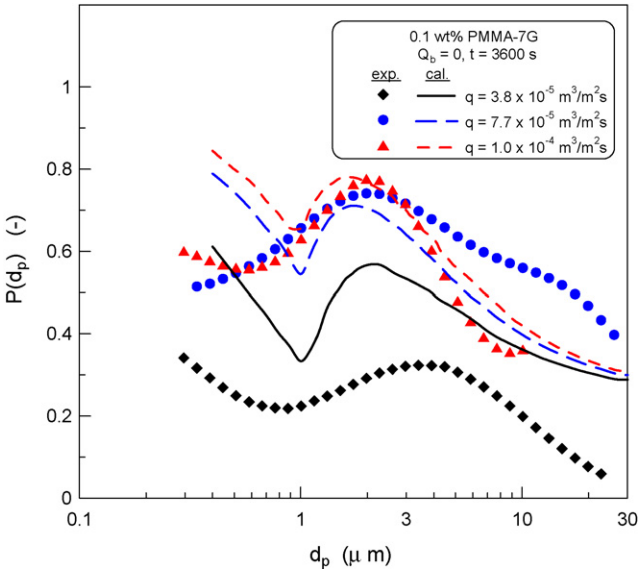

Fig. 7. Effect of filtration flux on the particle deposition probability.

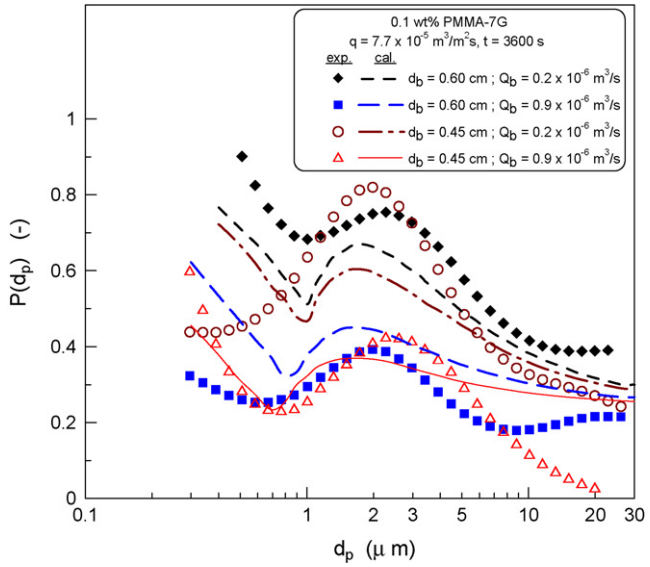

Fig. 8. Effects of air flow rate and bubble size on the particle deposition probability.

calculation can satisfactorily agree with experimental data under certain ranges of d_p. The deviation between calculated results and experimental data is less than 30% within the particle size range of 1–15 μm. However, large discrepancies occur when particle size is out of this range. It is possible due to few particles with those sizes existing in the particulate sample. The insufficient sample leads to a difficult size measurement. The data shown in Fig. 8 reveals that the air flow rate makes a greater impact on the particle deposition than the bubble size does. A higher air flow rate leads to lower particle deposition probability due to higher shear stress acting on the membrane surface. Although a bigger bubble is believed to generate a higher shear stress, the generation frequency is relatively lower for bigger bubbles under the same air flow rate. As a result, the particle deposition probabilities are similar for different size bubbles under the same air flow rate. In fact, only a slightly higher deposition probability can be observed for bigger bubbles (d_b = 0.6 cm).

Once the particle deposition probability is known, the cake mass can be calculated using Eq. (12). Fig. 9 shows a comparison of cake mass at 3600 s between calculated results and experimental data under various filtration fluxes. Since a higher filtration flux results in a larger drag force in the filtration direction, the particles on the membrane surface are more stable. Consequently, heavier cake is formed under a higher filtration flux. Comparing the data shown in Fig. 9, a good agreement between simulated results and experimental data is obtained. Only the cake mass formed under a low filtration flux is underestimated. It is because of the underestimation in the particle deposition probability in the early period of filtration.

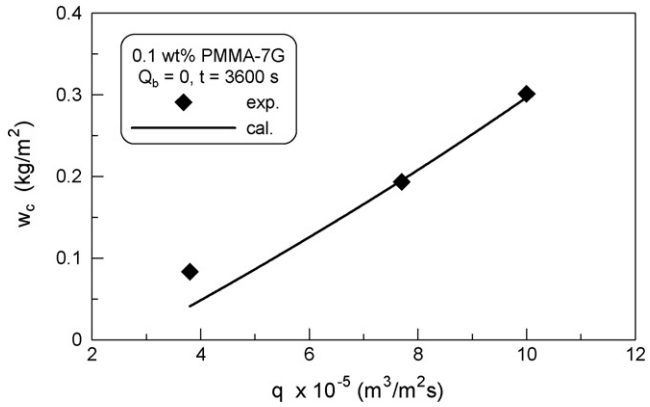

Fig. 9. Effect of filtration flux on the cake mass.

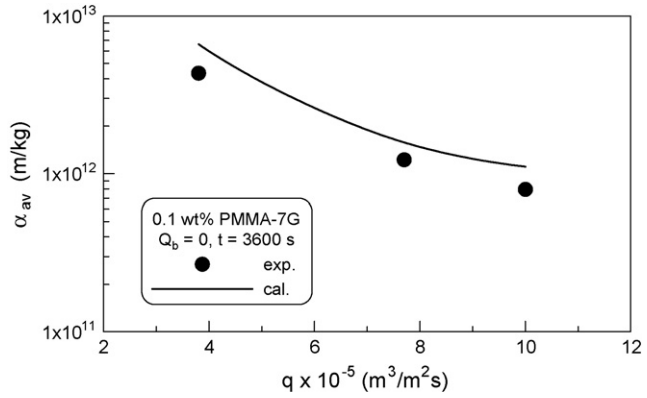

Fig. 10. Effect of filtration flux on the average specific cake filtration resistance.

The mean particle diameter in the cake under various conditions can be calculated once the particle deposition probability is known. Hence, the average specific cake filtration resistance, α_{av}, can be estimated using Eq. (14) in which the cake porosity and S_o are calculated using Eq. (13) and (6)/$d_{p,av}$, respectively. Fig. 10 shows the effect of filtration flux on the value of α_{av}. Since the particle size distribution is larger under higher filtration flux, as shown in Fig. 5, the larger mean diameter leads to a lower α_{av}. When filtration flux increases 2.5-fold from 3.8×10^{-5} to 1.0×10^{-4} m^3/m^{2}s, the value of α_{av} becomes only a half. It can be seen that both calculated and experimental α_{av} values have the same tendencies. However, the calculated α_{av} is higher than experimental data due to the underestimation of the mean particle size in cake.

Fig. 11 shows the effects of bubble size and air flow rate on the cake mass under a fixed filtration flux of 7.7×10^{-5} m^3/m^{2}s. The filtration times were all set at 3600 s. The cake accumulation is efficiently reduced by increasing air flow rate. The cake mass becomes only 20% when air volumetric flow rate increases from 0 to 0.9×10^{-6} m^3/s. Since the generation frequency is higher for injecting smaller bubbles under a given air flow rate, to inject smaller bubbles results in higher shear stress acting on the membrane surface. Therefore, the cake mass is lighter by injecting smaller bubbles under a given air flow rate. The figure also shows a fairly

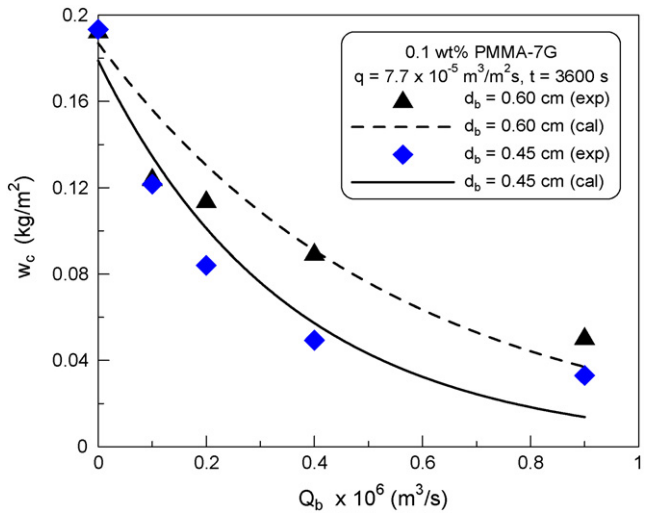

Fig. 11. Comparisons of cake mass between calculated results and experimental data under various air flow rates and bubble sizes.

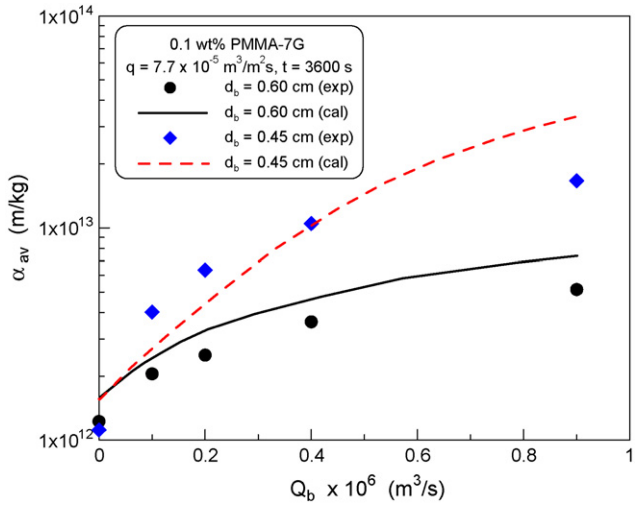

Fig. 12. Comparisons of average specific cake filtration resistance between calculated results and experimental data under various air flow rates and bubble sizes.

good agreement between calculated cake mass and experimental data.

Fig. 12 shows the comparisons of average specific cake filtration resistance between calculated results and experimental data under various bubble sizes and air flow rates. Since a higher air flow rate results in a smaller particle size distribution in the cake, the value of α_{av} increases with increasing air flow rate. This effect is more significant by injecting smaller bubbles. The α_{av} value may increases 2–10-fold by air bubble injection within the operating conditions of this study. An agreement between calculated results and experimental data can be seen when $Q_b \leq 0.4 \times 10^{-6}$ m^3/s. The overestimation in α_{av} values under high air flow rate is attributed to the overestimation in the deposition probability of submicron particles. The mean particle size in cake is thus underestimated. Considering those data shown in Figs. 11 and 12, increasing the bubble size under the same air flow rate is more efficient on the viewpoint of reducing overall cake resistance. Although injecting smaller bubbles can reduce more cake mass, the specific filtration resistance will become much higher.

5. Conclusions

The effects of operating conditions, such as filtration flux, injected air flow rate and air bubble size, on the particle deposition probability, cake mass and average specific cake filtration resistance in constant-flux submerged membrane filtration were discussed. The particle size distribution in the formed cake was smaller than that in the suspension and increased with increasing filtration flux. The drag forces due to suspension flow, permeate flow, and air bubble flow played the major roles on the particle deposition. Interparticle forces were dominant for submicron particles, while gravitational force increased its weight as particle size exceeded 5 μm. A force balance model for particle deposition was derived based on hydrodynamics and DLVO theory. Under a given operating condition, the deposition probability decreased with particle size and reached a minimum value for submicron particles, then increased until a maximum at a particle diameter *ca.* 2–3 μm, and finally decreased with particle size for larger micron particles. This trend could be explained using the force analysis and was verified by experimental data. An increase in filtration flux or a decrease in air flow rate led to a higher particle deposition probability, a heavier cake mass, or lower average specific cake filtration resistance. The deposition probability was higher by injecting bigger bubbles under the same air flow rate due to the lower bubble generation frequency. Consequently, decreasing bubble size caused thinner cake but higher specific filtration resistance. According to Kozeny equation with $k = 5.0$, the cake mass and average specific filtration resistance under various conditions were calculated theoretically and compared with experimental data. The deviation between calculated results and experimental data was less than 30% within the particle size range of 1–15 μm.

Acknowledgements

The authors wish to express their sincere gratitude to the National Science Council of the Republic of China for its financial support.

References

[1] G. Belfort, R.H. Davis, A.L. Zydney, The behavior of suspensions and macromolecular solutions in crossflow microfiltration, J. Membr. Sci. 96 (1994) 1–58.
[2] Z.F. Cui, S. Chang, A.G. Fane, The use of gas bubbling to enhance membrane process, J. Membr. Sci. 221 (2003) 1–35.
[3] J.H. Kim, F.A. DiGiano, Particle fouling in submerged microfiltration membranes: effects of hollow-fiber length and aeration rate, J. Water Supply: Res. Technol. Aqua 55 (7–8) (2006) 535–547.
[4] K.J. Hwang, F.F. Chen, Modeling of particle fouling and membrane blocking in submerged membrane filtration, Sep. Sci. Technol. 42 (12) (2007) 2595–2614.
[5] S. Chang, A.G. Fane, The effect of fibre diameter on filtration and flux distribution—relevance to submerged hollow fibre modules, J. Membr. Sci. 184 (2001) 221–231.
[6] A.G. Fane, S. Chang, E. Chardon, Submerged hollow fibre membrane module—design options and operational considerations, Desalination 146 (2002) 231–236.
[7] W.M. Lu, S.C. Ju, Selective particle deposition in cross-flow filtration, Sep. Sci. Technol. 24 (7,8) (1989) 517–540.
[8] W.M. Lu, K.J. Hwang, Cake formation in 2-D cross-flow filtration, AIChE. J. 41 (6) (1995) 1443–1455.
[9] G. Foley, D.M. Malone, F. MacLoughlin, Modelling the effects of particle polydispersity in crossflow filtration, J. Membr. Sci. 99 (1995) 77–88.
[10] K.J. Hwang, Y.L. Hsu, K.L. Tung, Effect of particle size on the performance of cross-flow microfiltration, Adv. Powder Technol. 17 (2) (2006) 189–202.
[11] M.E. O'Neill, A sphere in contact with a plane wall in slow linear shear flow, Chem. Eng. Sci. 23 (1968) 1293–1297.
[12] J.D. Sherwood, The force on a sphere pulled away from a permeable half-space, Physicochem. Hydrodyn. 10 (1988) 3–12.
[13] P. Vasseur, R.G. Cox, The laterial migration of spherical particle in two dimensional shear flow, J. Fluid Mech. 78 (1976) 385–413.
[14] K.J. Hwang, H.C. Liu, W.M. Lu, Local properties of cake in cross-flow microfiltration of submicron particles, J. Membr. Sci. 138 (1998) 181–192.
[15] L.S. Fan, K. Tsuchiya, Bubble Wake Dynamics in Liquids and Liquid-Solid Suspensions, Butterworth-Heinemann, Stoneham, MA, USA, 1990, Chap. 2, pp. 17–69.
[16] D.F. Evans, H. Wennerström, The Colloidal Domain, 2nd ed., Wiely–VCH, NY, USA, 1999, Chap. 5.